



Research Article

Three dimensional flow over elliptic cylinders arrays in octagonal arrangement

Rajesh KUMAR^{1,*}, Nirmal KANT SINGH¹

¹Department of Mechanical Engineering, National Institute of Technology, Kurukshetra, Haryana, India

ARTICLE INFO

Article history

Received: 14 June 2020

Accepted: 09 August 2020

Key words:

Array attack angle; Vortex shedding; Drag and lift forces; Gap spacings

ABSTRACT

A numerical study of flow characteristics around eight elliptic cross-section cylinders in an octagonal configuration is presented. The axis ratio of elliptic cylinder is taken as 1:2. Three spacings between the cylinders (0.07 m, 0.14 m and 0.2 m), two angles of attack ($\alpha=0^\circ$ and $\alpha=15^\circ$) and two Reynolds numbers ($Re=4060$ and $Re=45800$) are considered to investigate the parametric influences. The flow is modelled using three-dimensional large eddy simulation. Simulations are performed by utilizing ANSYS Fluent software. The results comprise of flow patterns and force coefficients (drag and lift). It is seen that both the drag and lift forces acting on the cylinders vary with the spacings values, angle of attack and Reynolds numbers. The lift force peaks at $\alpha=15^\circ$ and Reynolds number 45800. The drag force on the upstream cylinder reaches its peak at $\alpha=0^\circ$ and Reynolds number 4060. It is observed that the drag on the upstream cylinders decreases as the value of the Reynolds number increases. Contours of velocity and subgrid turbulent viscosity are also presented. Moreover, it is concluded from the present study that the effect of change in the Reynolds number on flow characteristics is more significant as compared to the change in the spacing between the cylinders.

Cite this article as: Kumar R, Kant Singh N. Three dimensional flow over elliptic cylinders arrays in octagonal arrangement. J Ther Eng 2021;7(Supp 14):2031–2040.

INTRODUCTION

Fluid interaction with multiple bluff bodies has gained much significance because of its various applications in diverse fields of engineering. Some familiar examples are nuclear rods, heat exchangers, condensers, boilers etc. Drummond and Tahir [1] found the solutions for fluid past arrays of cylinders with different arrangements of cylinders.

The different arrangements of cylinders taken were square, triangular and rectangular. The direction of flow taken was perpendicular to the cylinder axes. Donald and Anthony [2] investigated the pressure drop required for the fluid to flow through arrays of randomly aligned cylinders. Zou and Lin [3] found that the cylinders in the downstream direction experience lower forces than the cylinders which are placed in the upstream direction of the fluid flow. Alternate

*Corresponding author.

*E-mail address: rajesh.me.sb@gmail.com

This paper was recommended for publication in revised form by Regional Editor Erman Aslan



wide and narrow wakes are generated at different instants of time. Different values of drag and lift force coefficients values were obtained for the arrays of cylinders considered for the numerical simulation.

Liu et al. [4] conducted a visualization study for the variation in fluid flow characteristics and behaviour of a plate placed at a certain angle to the fluid flow direction. They investigated the flow for various values of angle of attack and found changes in the flow characteristics with the change in the angle of attack. Han et al. [5] studied numerically flow over four cylinders arranged in square configuration. The method used for the study was the spectral element method. The simulation results obtained showed that the effect on the force coefficients is high with the changes in the flow patterns. Liu et al. [6] studied experimentally flow past arrays of four square cylinders in a square arrangement at subcritical Reynolds number. They found the values of drag and lift coefficients for various spacing ratios and angles of attack.

Qadi et al. [7] presented three-dimensional large-eddy simulation (LES) of flow around two circular cylinders in tandem placed in an open channel. The three-dimensional flow characteristics were investigated with the help of the results obtained from LES. Chang and Constantinescu [8] numerically investigated circular cylinder arrays. Various ways were presented for explaining the changes in the formation of the wake regions formed. Tong et al. [9] investigated numerically flow over two similar circular cylinders arranged in various configurations. They conducted their study at a low Reynolds number, $Re=1000$. Two different vortex shedding frequencies were identified, which were caused due to the gap differences in the wake region formed when the fluid flows across the array of cylinders. Islam et al. [10] studied the effect of the spacing between the cylinders numerically. Three cylinders were arranged in tandem configuration. The values of the mean drag and lift coefficients were found. A critical value of gap spacing was found. Koide et al. [11] numerically studied the flow over two cylinders with different cross-sections. They studied the vortex shedding characteristics for the fluid flow across the cylinders. They observed different frequencies of vortex shedding for the case investigated. Fayed et al. [12] did the visualization and simulation studies for the two-dimensional flow of fluid over a foil. They compared the visualization results with the numerical simulation results. Alizadeh et al. [13] numerically investigated the dynamic behaviour of the beams under impulsive fluid force. A commercial finite element code is applied for the investigation.

Islam et al. [14] numerically simulated flow over seventeen square cross-section cylinder array using lattice Boltzmann method in two-dimensional flow configuration. The cylinders were arranged in a staggered arrangement, and the investigation was done at different spacings between the cylinders. Kim et al. [15] performed a numerical simulation of flow past a cylinder inclined at an angle of 45° .

The value of Reynolds number used was 11,800. Chamoli et al. [16] investigated numerically for the flow across a cam shaped cylinder. It was found that the heat transfer increases and drag decreases for the investigated shape of the cylinder when compared with other bluff bodies.

Zhou et al. [17] experimentally investigated for the variations of drag coefficients with and without splitter plate were investigated. Sun et al. [18] investigated the interaction between the vortex and surface experimentally in the streamwise direction. Various contours of vortex formation were obtained. The vortex generated near the wall surface known as a primary vortex causes secondary vortex formation. The parameters which affect the flow field characteristics are the distance between the surface and the vortex core and the strength of the primary vortex formed. Gao et al. [19] performed numerical simulations in two-dimensional of the flow over six cylinders arranged in a configuration of a 2×3 matrix and a configuration of a 3×2 matrix. The simulations were presented at a low Reynolds number. The power spectral density plots were observed having multiple peaks. The Strouhal numbers values were obtained from the power spectral density plots for the six-cylinders array investigated. Sefiddashti et al. [20] numerically studied flow over an airfoil at a subcritical value of Reynolds number. Riblets were also attached with the airfoil. It was found that the size of the wake changed with the size of the riblets. Ferrari et al. [21] obtained a new approach for visualizing the vortex formation characteristics. The visualization was done for various vortex shedding cycles. They found the approach helpful for making further comparisons which were not available in the traditional visualization techniques. Yun et al. [22] experimentally studied for the flow past two spheres placed in tandem configuration. Grioni et al. [23] numerically simulated flow past two circular cross-section cylinders in a tandem arrangement. The turbulence model used for performing the numerical simulations was Scale-Adaptive Simulations (SAS). The high sub-critical value of Reynolds number used was 2×10^5 . The simulations were performed for various values of the distance between the cylinders. The spacing ratio L/D varies from the range of 1.1 to 7, where D is the cylinder diameter. A critical value of the spacing ratio between the cylinders was obtained at $L/D=3$. The present study aims to numerically simulate the flow over eight elliptic cylinder arrays placed in octagonal arrangement using large-eddy simulation.

METHODOLOGY

Computational Flow Domain

The geometry of the problem studied is shown in Fig. 1 which is created in ANSYS 19R1 Design modeller. It consists of a rectangular flow domain having eight elliptic cylinders of hydraulic diameter D_c , 0.029 m and axis ratio a/b , 1:2 arranged in an octagonal configuration. Three spacings

between the cylinders, i.e. length of the side of the octagonal, $L=0.07$ m, 0.14 m and 0.2 m, two array attack angle, $\alpha=0^\circ$, 15° and two Reynolds number, $Re=4060$, 45800 are considered for the numerical investigation. Effect of the spacing (L) is explored via the creation of three geometries, which are $L=0.07$ m, 0.14 m and 0.2 m. Also, the effect of the arrays attack angle (α) is investigated by altering the angle of attack in the geometry from 0° to 15° . Moreover, the effect of the Reynolds number (Re) is also studied by increasing the Reynolds number from 4060 to 45800 . The working fluid used is air which has the following properties: density, $\rho=1.225$ kg/m³, kinematic viscosity, $\nu = 1.48 \times 10^{-5}$ m²/s. The computational domain for the investigated parameters is shown in Figs. 2, 3, and 4, respectively.

Governing Equations of Flow

Three-dimensional Continuity Equation

$$\frac{\partial u}{\partial x} + \frac{\partial v}{\partial y} + \frac{\partial w}{\partial z} = 0 \tag{1}$$

Three-dimensional Momentum Equation

x-momentum equation:

$$\frac{\partial u}{\partial t} + u \frac{\partial u}{\partial x} + v \frac{\partial u}{\partial y} + w \frac{\partial u}{\partial z} = -\frac{1}{\rho} \frac{\partial p}{\partial x} + \nu \left(\frac{\partial^2 u}{\partial x^2} + \frac{\partial^2 u}{\partial y^2} + \frac{\partial^2 u}{\partial z^2} \right) \tag{2}$$

y-momentum equation:

$$\frac{\partial v}{\partial t} + u \frac{\partial v}{\partial x} + v \frac{\partial v}{\partial y} + w \frac{\partial v}{\partial z} = -\frac{1}{\rho} \frac{\partial p}{\partial y} + \nu \left(\frac{\partial^2 v}{\partial x^2} + \frac{\partial^2 v}{\partial y^2} + \frac{\partial^2 v}{\partial z^2} \right) \tag{3}$$

z-momentum equation:

$$\frac{\partial w}{\partial t} + u \frac{\partial w}{\partial x} + v \frac{\partial w}{\partial y} + w \frac{\partial w}{\partial z} = -\frac{1}{\rho} \frac{\partial p}{\partial z} + \nu \left(\frac{\partial^2 w}{\partial x^2} + \frac{\partial^2 w}{\partial y^2} + \frac{\partial^2 w}{\partial z^2} \right) \tag{4}$$

Meshing- Grid Generation

The geometry of the problem studied is created by the computer tool ICEM CFD (Integrated Computer Engineering and Manufacturing). The computational

domain is meshed by hexahedral grid elements. A control volume approach is used for the discretization of the governing equations. A refined mesh near the elliptic cylinder wall was created to capture details of the hydrodynamic boundary layer. The selected mesh grid had about 2.1 million of elements. Figs. 5, 6 and 7 show the quality of the mesh used for the three spacings, L (i.e. 0.07 m, 0.14 m and 0.2 m) and two angles of attack, α (i.e. 0° and 15°) respectively. Figure 8 shows the grid created around an elliptic cylinder.

Numerical Details

A uniform inlet velocity is used, and for the walls of the cylinders, the no-slip boundary condition is applied. All axial derivatives are considered to be zero at the exit of the flow domain, i.e. the fully developed flow assumption is used. The side surfaces of the flow domain are considered to be symmetric. A constant turbulence intensity of 0.7% is employed. The commercial software ANSYS (version 19R1) was used to conduct all the computations. The SIMPLE

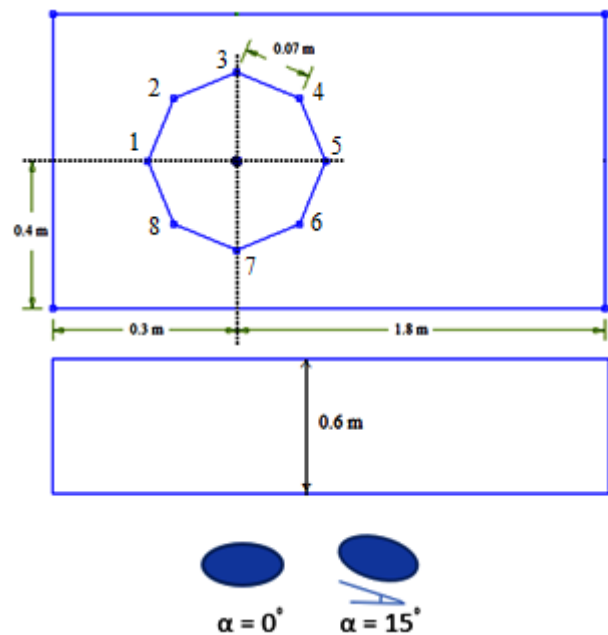


Figure 1. Computational flow domain dimensions.

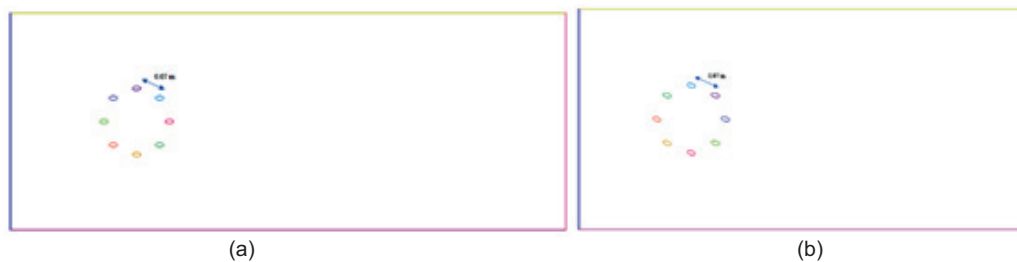


Figure 2. Geometry for 0.07 m spacing, (a) $\alpha = 0^\circ$ and (b) $\alpha = 15^\circ$.

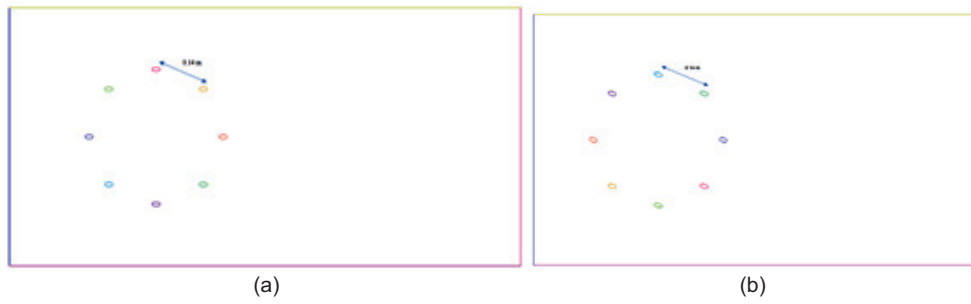


Figure 3. Geometry for 0.14 m spacing, (a) $\alpha = 0^\circ$ and (b) $\alpha = 15^\circ$.

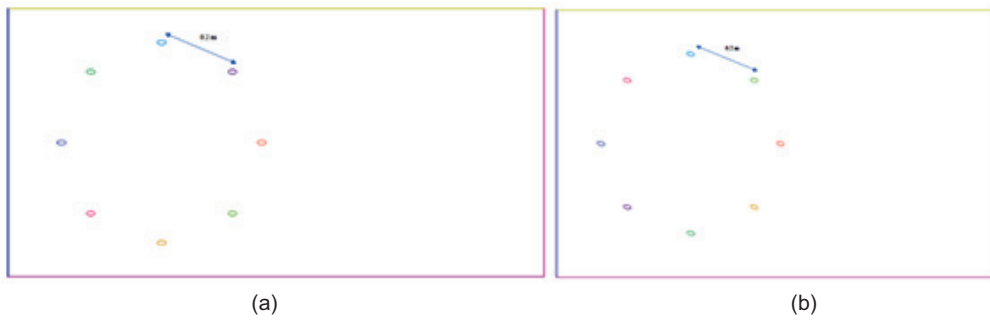


Figure 4. Geometry for 0.2 m spacing, (a) $\alpha = 0^\circ$ and (b) $\alpha = 15^\circ$.

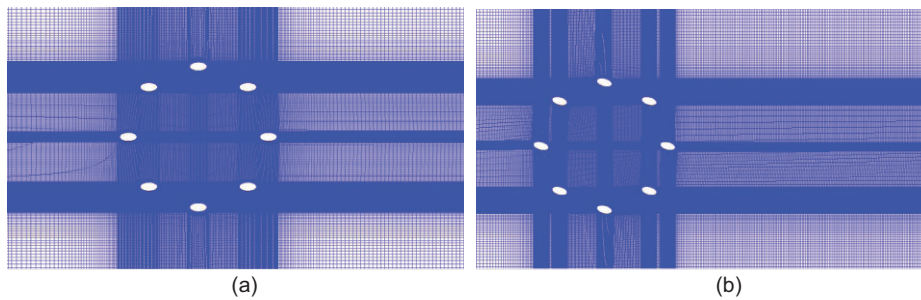


Figure 5. Mesh created for 0.07 m spacing, (a) $\alpha = 0^\circ$ and (b) $\alpha = 15^\circ$.

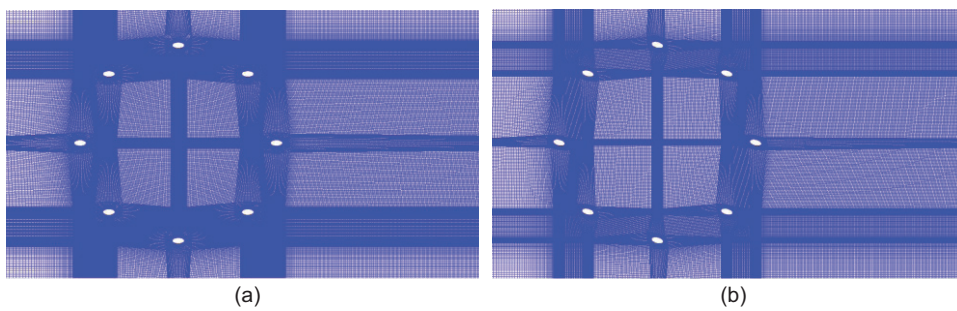


Figure 6. Mesh created for 0.14 m spacing, (a) $\alpha = 0^\circ$ and (b) $\alpha = 15^\circ$.

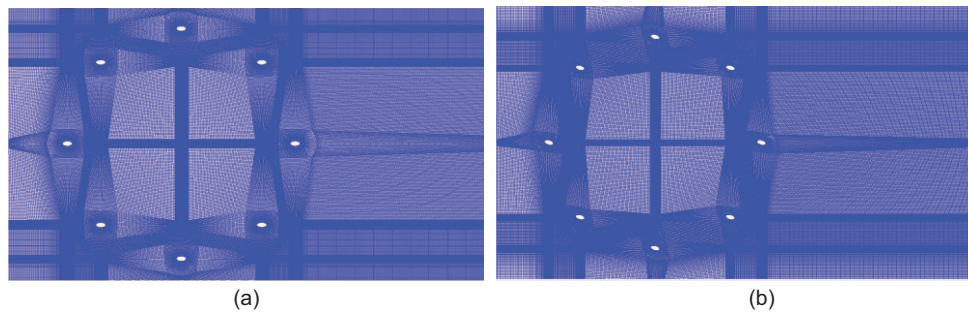


Figure 7. Mesh created for 0.2 m spacing, (a) $\alpha = 0^\circ$ and (b) $\alpha = 15^\circ$.

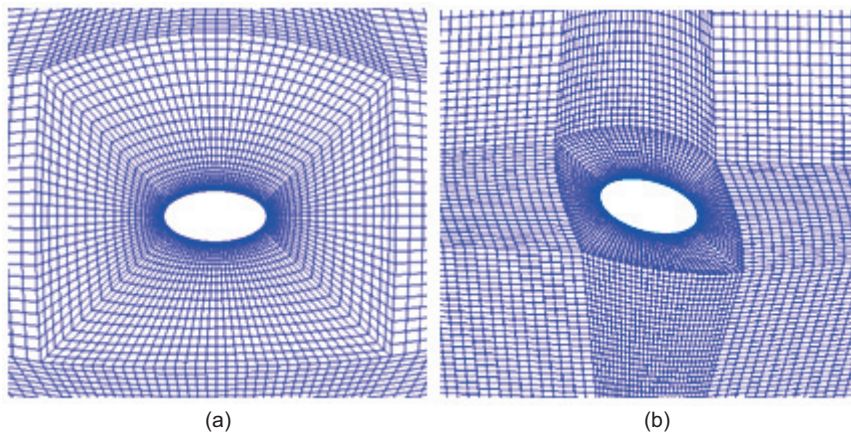


Figure 8. Grid created near the surface of the cylinder, (a) $\alpha = 0^\circ$ and (b) $\alpha = 15^\circ$.

(Semi Implicit Method for Pressure Linked Equation) algorithm was used to perform pressure-velocity coupling. Least squares cell-based technique is utilized for gradient evaluation. Pressure interpolation is done with the help of a second-order interpolation scheme. For obtaining precision of the transient formulation, bounded second-order implicit scheme was adopted. To ensure the convergence, the following under-relaxation factors were set for the pressure, density, body forces and momentum respectively: 0.3, 1, 1 and 0.7. The residual target was set to 10^{-6} for the continuity, x, y and z momentum equations. The time histories of drag and lift coefficients were monitored for the onset of periodicity in the flow calculations. In the present study simulation is done at two Reynolds number, i.e. 4060 and 45800. The time step size chosen for Reynolds number 4060 is 1×10^{-5} and for 45800 is 1×10^{-7} .

Validation

To confirm the reliability of the computer code, and the accuracy of the numerical method undertaken, validation of some obtained results was carried out. For this purpose, the experimental work of Liu et al. [6] was referred. The experimental work was done on four cylinders arranged in a square configuration. Figure 9 shows the comparison of the mean drag and lift coefficients found experimentally by Liu et al. [6] and numerically in the present work for each

of the four cylinders. The experiment was carried out in a closed low speed wind tunnel with 0.7% turbulence intensity. Our predicted results for the mean drag and lift coefficients are presented in Fig. 9. As observed, the validation shows a satisfactory agreement.

RESULTS AND DISCUSSION

The effect of different spacings between the cylinders, variation in the array attack angle and altering the Reynolds number is examined in this section. Contours of various quantities were obtained from the numerical simulation performed such as velocity magnitude contours, subgrid turbulent viscosity contours, velocity contours in stream-wise and transverse directions. The effect of flow domain dimensions on the time histories of the drag coefficient and lift coefficient is also discussed in this section.

Effect of Spacing Between the Cylinders (L)

In this section, an investigation into the effects of the spacings between the cylinders is made. Three spacings are considered which are: $L=0.07$ m, 0.14 m and 0.2 m. It was observed that the mean force coefficients vary for different spacings between the cylinders. Mean drag and lift coefficients are shown in Fig. 10 and Fig. 11 for Reynolds number 4060 and 45800, respectively.

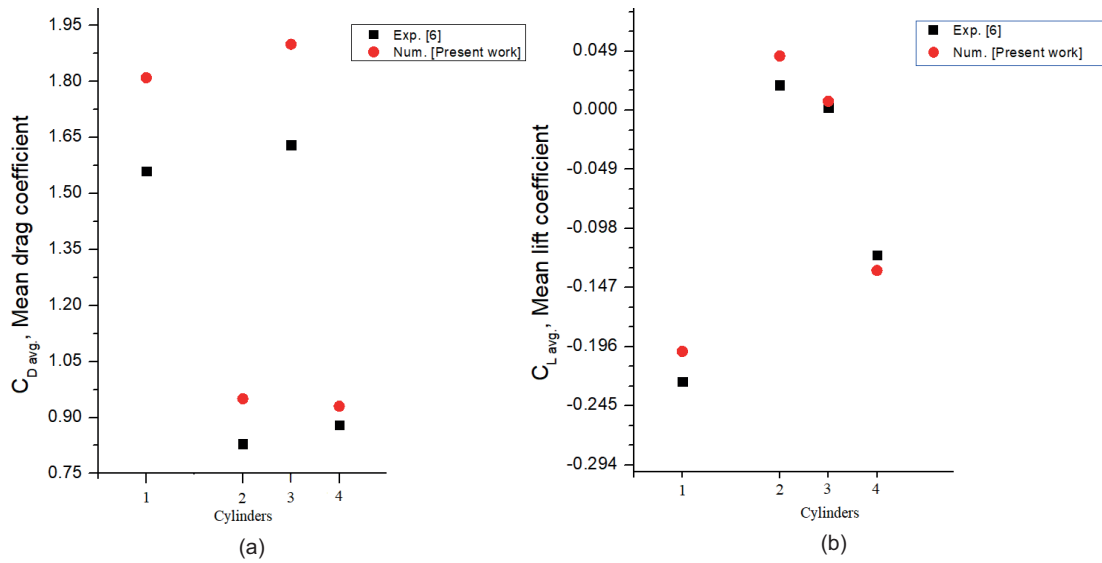


Figure 9. Comparison of numerical results from the present work with experimental data of [6] for (a) mean drag coefficient (b) mean lift coefficient.

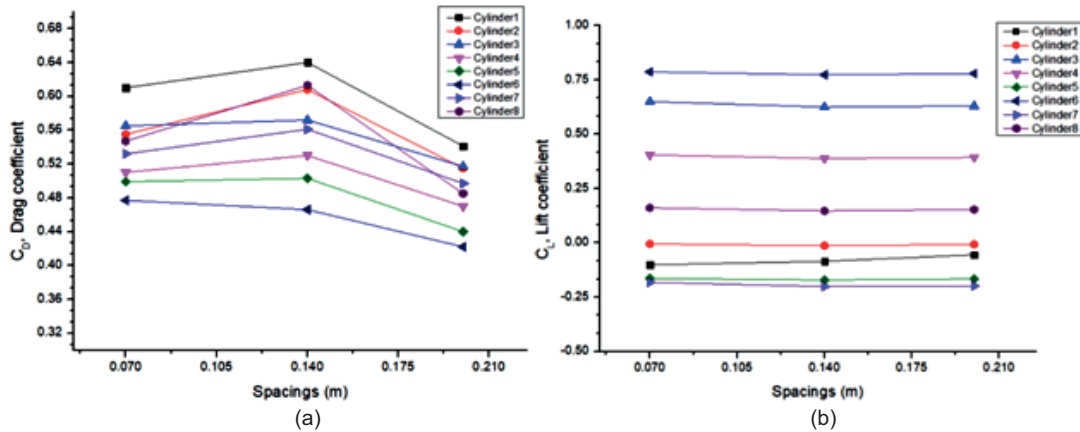


Figure 10. (a) Average drag coefficient, (b) Average lift coefficient [Re = 4060].

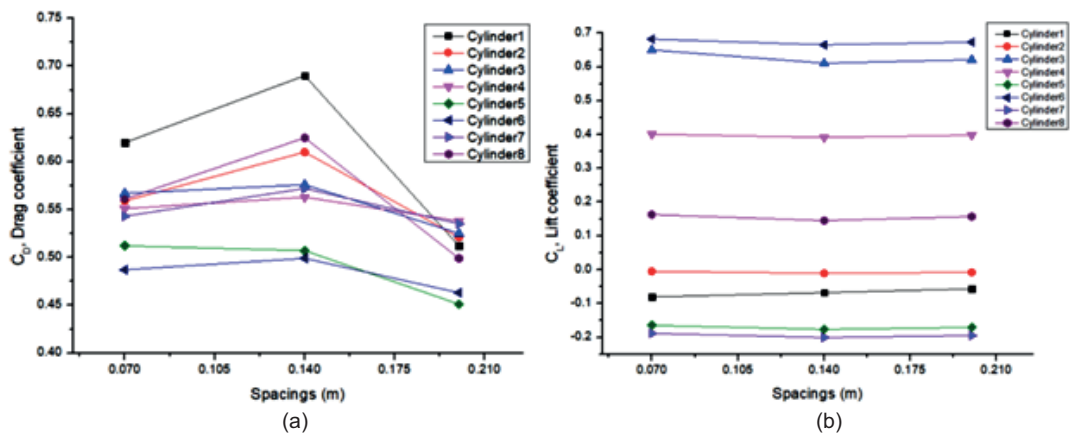


Figure 11. (a) Average drag coefficient, (b) Average lift coefficient [Re = 45800].

Effect of the Reynolds Number (Re)

The effect of the Reynolds number on the force coefficients is discussed in this section. The values of the mean force coefficients at two different Reynolds number 4060 and 45800 obtained in our numerical simulation are shown in Table 1 and Table 2. The value of the drag coefficient for upstream cylinders is higher when compared with the downstream cylinders. The reason for this is that the fluid directly impinges on the upstream cylinders and has more pressure drag. Another observation is that the drag is decreasing with the increase of the Reynolds number. It is due to the flow separation that moves towards the downstream side of the cylinders. Moreover, it was also observed that the effect of Reynolds number is higher on the flow characteristics compared to the effect of spacing between the cylinders.

Effect of the Angle of Attack (α)

The impact of another geometrical parameter is analyzed in this section; it concerns the arrays' attack angle (α). Two geometrical configurations were realized to carry out the study, which are: $\alpha=0^\circ$ and $\alpha=15^\circ$. The results for the investigated angles are shown in the form of contours. It was observed that the size of the vortices developed behind the cylinder is greater for $\alpha=0^\circ$ as compared with the size at $\alpha=15^\circ$ because of the decrease in the intensity of the axial

component of velocity with the increase of the arrays attack angle. Non-symmetrical vortex formation is observed on upward and downward sides of the cylinders at $\alpha=15^\circ$ compared to the symmetrical vortex formation at $\alpha=0^\circ$. More observations on the discussed effects can be seen from the various contours of velocity and viscosity at both the angles shown in Figs. 12, 13 and 14 obtained from our numerical investigation. The time histories of the drag coefficient and lift coefficient are also shown in Fig. 15.

CONCLUSIONS

The present study has allowed a three-dimensional visualization of hydrodynamic fields around the array of cylinders. Effect of the spacing (L) between the cylinders has been explored. It is found that the cylinder which is in side-by-side position in an octagonal configuration experiences approximately similar mean drag and lift forces as the spacing ratio increases. The array attack angles (α) used for the investigation were 0° and 15° . It was found that at $\alpha=0^\circ$, the drag force on the downstream cylinders is moderately less than that on the upstream cylinders. The downstream cylinder reaches its maximum lift force and experiences lower drag at $\alpha=15^\circ$. Concerning the effect of the Reynolds number, which plays a major role in the variation of flow features, it was found that at higher Reynolds number

Table 1. Mean force coefficients at Re = 4060 and $\alpha = 0^\circ$

| Spacings, L (m) | Cylinder | $(C_D)_{avg.}$ | $(C_L)_{avg.}$ |
|-----------------|----------|----------------|----------------|
| L = 0.07 | 1 | 0.610 | -0.101 |
| | 2 | 0.555 | -0.005 |
| | 3 | 0.565 | 0.750 |
| | 4 | 0.510 | 0.405 |
| | 5 | 0.499 | -0.164 |
| | 6 | 0.477 | 0.787 |
| | 7 | 0.532 | -0.182 |
| | 8 | 0.547 | 0.161 |

Table 2. Mean force coefficients at Re = 45800 and $\alpha = 0^\circ$

| Spacings, L (m) | Cylinder | $(C_D)_{avg.}$ | $(C_L)_{avg.}$ |
|-----------------|----------|----------------|----------------|
| L = 0.07 | 1 | 0.590 | -0.104 |
| | 2 | 0.552 | -0.008 |
| | 3 | 0.561 | 0.625 |
| | 4 | 0.490 | 0.399 |
| | 5 | 0.497 | -0.184 |
| | 6 | 0.475 | 0.675 |
| | 7 | 0.530 | -0.199 |
| | 8 | 0.545 | 0.152 |

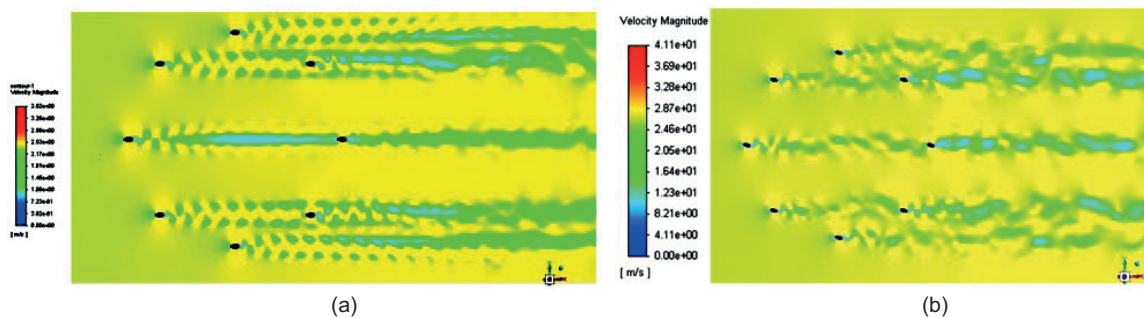


Figure 12. Velocity magnitude contours at (a) $\alpha = 0^\circ$, (b) $\alpha = 15^\circ$.

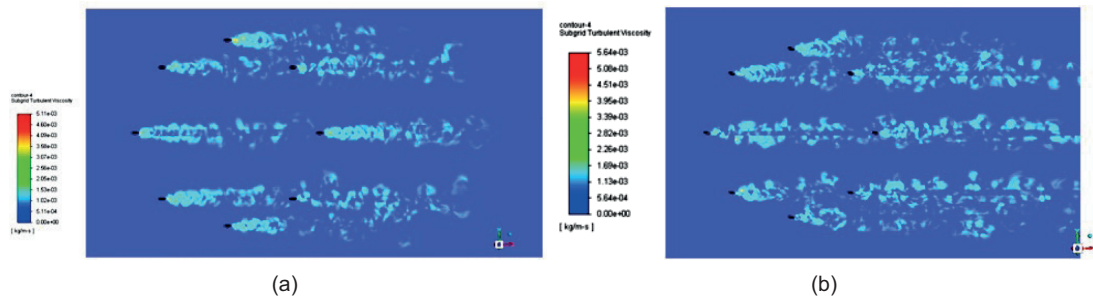


Figure 13. Subgrid turbulent viscosity contours at (a) $\alpha = 0^\circ$, (b) $\alpha = 15^\circ$.

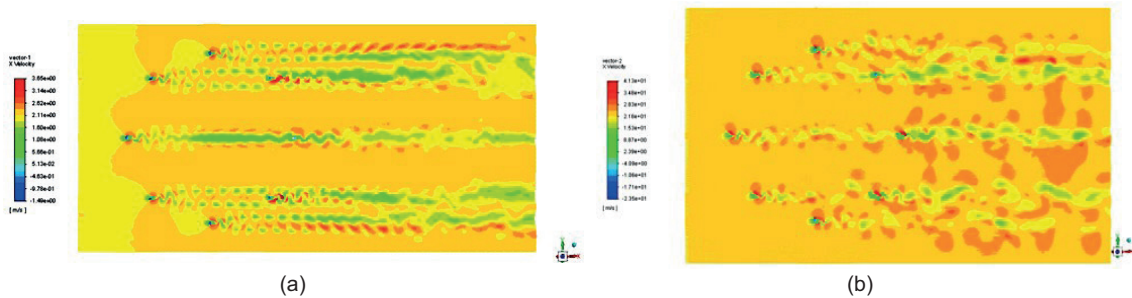


Figure 14. Streamwise velocity magnitude contours at (a) $\alpha = 0^\circ$, (b) $\alpha = 15^\circ$.

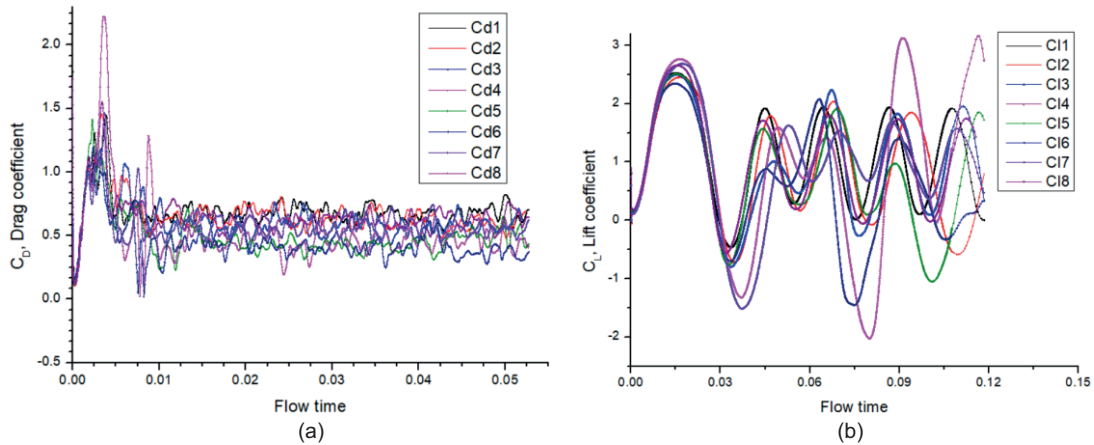


Figure 15. (a) Time histories of drag variation with flow time, (b) Time histories of lift variation with flow time.

mean drag force on the cylinders decreases but resulted in the enhancement of the mean lift forces. The comparison of effects of Reynolds number and the gap spacing shows that the impact of the Reynolds number on the vortex shedding mechanism dominates the effect of the gap spacing. The obtained results confirm that the mean drag coefficient reduces in the streamwise direction for a fixed Reynolds number and gap spacing. Moreover, the chaotic flow regime is the most observed flow regime for the investigated configuration.

NOMENCLATURE

- A_p area projected (m^2)
- a, b elliptic cylinders major and minor axes (m)
- a/b axis ratio
- C_D coefficient of drag ($= F_x / (0.5 * \rho U_\infty^2 A_p)$)
- C_L coefficient of lift ($= F_y / (0.5 * \rho U_\infty^2 A_p)$)
- C_s model constant (Smagorinsky)
- D_e hydraulic diameter (m)
- L_c characteristic length (m)

L spacing between elliptic cylinders (m)
 U_{∞} velocity (m/s)
 Re ($=U_{\infty}D/\nu$) Reynolds number

Greek symbols

ρ density (kg/m^3)
 ν kinematic viscosity (m^2/s)
 α angle

AUTHORSHIP CONTRIBUTIONS

Authors equally contributed to this work.

DATA AVAILABILITY STATEMENT

The authors confirm that the data that supports the findings of this study are available within the article. Raw data that support the finding of this study are available from the corresponding author, upon reasonable request.

CONFLICT OF INTEREST

The author declared no potential conflicts of interest with respect to the research, authorship, and/or publication of this article.

ETHICS

There are no ethical issues with the publication of this manuscript.

REFERENCES

- [1] Drummond JE, Tahir MI. Laminar viscous flow through regular arrays of parallel solid cylinders. *Int J Multiphase Flow* 1984;10:515–540. [\[CrossRef\]](#)
- [2] Donald LK, Anthony JCL. Moderate Reynolds number flows through periodic and random arrays of aligned cylinders. *J Fluid Mech* 1997;349:31–66. [\[CrossRef\]](#)
- [3] Zou L, Lin Y.F. Bistable flow pattern for cylinder arrays with a small spacing ratio. *J Vis* 2009;12:193–194. [\[CrossRef\]](#)
- [4] Liu Y, Yang WC, Yang JM. A visualization study of the near-wall behaviours of an oblique plate at different angles of attack. *J Vis* 2011;14:141–148. [\[CrossRef\]](#)
- [5] Han Z, Zhou D, Gui X, Tu J. Numerical study of flow past four square-arranged cylinders using the spectral element method. *J Comput Fluids* 2013;84:100–112. [\[CrossRef\]](#)
- [6] Liu M, Xiao L, Yang L. Experimental investigation of flow characteristics around four square-cylinder arrays at subcritical Reynolds numbers. *Int J Nav Archit Ocean Eng* 2015;7:906–919. [\[CrossRef\]](#)
- [7] Qadi AI, Hazmy AM, Bahi AA, Rodi W. Large-eddy simulation of flow past tandem cylinders in a channel. *Flow Turbul Combust* 2015;95:621–643. [\[CrossRef\]](#)
- [8] Chang K, Constantinescu G. Numerical investigation of flow and turbulence structure through and around a circular array of rigid cylinders. *J Fluid Mech* 2015;776:161–199. [\[CrossRef\]](#)
- [9] Tong F, Cheng L, Zhao M. Numerical simulations of steady flow past two cylinders in staggered arrangements. *J Fluid Mech* 2015;765:114–149. [\[CrossRef\]](#)
- [10] Islam SU, Abbasi WS, Rahman H, Naheed R. Numerical investigation of wake modes for flow past three tandem cylinders using the multi-relaxation-time lattice Boltzmann method for different gap spacings. *J Braz Soc Mech Sci Eng* 2016;38:799–812. [\[CrossRef\]](#)
- [11] Koide M, Takahashi T, Shirakashi M, Salim SAZBS. Three-dimensional structure of longitudinal vortices shedding from cruciform two-cylinder systems with different geometries. *J Vis* 2017;20:753–763. [\[CrossRef\]](#)
- [12] Fayed M, Abderrahmane HA, Ng HD. Flow visualization and numerical simulation of two-dimensional fluid flow over a foil. *J Vis* 2017;20:687–693. [\[CrossRef\]](#)
- [13] Alizadeh MS, Shirazi KH, Moradi S, Sedighi HM. Numerical analysis of the counter-intuitive dynamic behaviour of the elastic-plastic pin-ended beams under impulsive loading with regard to linear hardening effects. *J Mech Eng Sci* 2018;232:1–13. [\[CrossRef\]](#)
- [14] Islam SU, Nazeer G, Ying ZC. Numerical investigation of flow past 17-cylinder array of square cylinders. *AIP Advances* 2018;8:065004. [\[CrossRef\]](#)
- [15] Kim M, Karbasian HR, Yeom E. Transient three-dimensional flow structures of oblique jet impingement on a circular cylinder. *J Vis* 2018;21:397–406. [\[CrossRef\]](#)
- [16] Chamoli S, Tang T, Peng Yu, Ruixin Lu. Effect of shape modification on heat transfer and drag for fluid flow past a cam-shaped cylinder. *Int J Heat Mass Transf* 2019;131:1147–1163. [\[CrossRef\]](#)
- [17] Zhou X, Wang JJ, Hu Y. Experimental investigation on the flow around a circular cylinder with upstream splitter plate. *J Vis* 2019;22:683–695. [\[CrossRef\]](#)
- [18] Sun Z, Gu Y, Zhao H. Experimental investigation on the streamwise vortex-surface interaction. *J Vis* 2019;22:477–488. [\[CrossRef\]](#)
- [19] Gao Y, Chen W, Wang B, Wang L. Numerical simulation of the flow past six-circular cylinders in rectangular configurations. *J Marine Sci Technol* 2020;25:718–742. [\[CrossRef\]](#)
- [20] Sefiddashti MN, Ahmadi MN, Rizi BS, Pourhoseini J. Visualization of flow over a thick

- airfoil with circular cross-sectional riblets at low Reynolds numbers. *J Vis* 2019;22:877–888. [[CrossRef](#)]
- [21] Ferrari S, Hu Y, Morton C, Martinuzzi RJ. Visualizing three-dimensional vortex shedding through evolution surface clusters. *J Vis* 2020;23:17–34. [[CrossRef](#)]
- [22] L Yun H, Lyu X, Wei Z. Experimental study on angled water entry of two tandem spheres with collision effect. *J Vis* 2020;23:49–59. [[CrossRef](#)]
- [23] Grioni M, Elaskar A, Mirasso AE. A numerical study of the flow interference between two circular cylinders in tandem by the scale-adaptive simulation model. *J Appl Fluid Mech* 2020;13:169–183. [[CrossRef](#)]